ChemComm

Accepted Manuscript

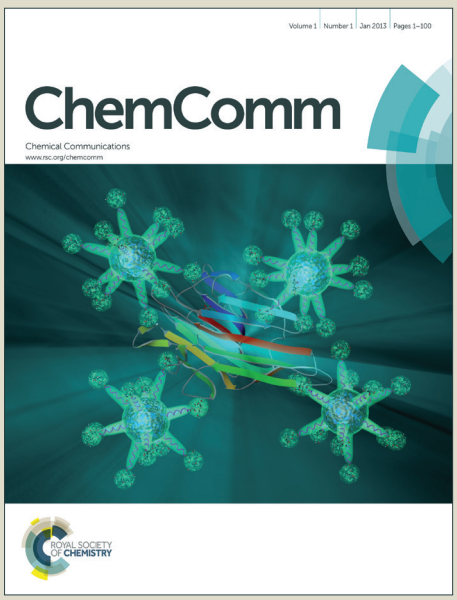

ROYAL SOCIETY OF CHEMISTRY

www.rsc.org/chemcomm

ChemComm

RSCPublishing

COMMUNICATION

Synthesis, Structure and Dehydrogenation of Zirconium Borohydride Octaammoniate

Cite this: DOI: 10.1039/xoxxoooooox

Jianmei Huang[a], Yingbin Tan[b], Jiahao Su[b], Qinfen Gu[c], Radovan Černý[d], Liuzhang Ouyang[a*], Dalin Sun[b], Xuebin Yu[b*], Min Zhu[a]

Received ooth January 2014,
Accepted ooth January 2014

DOI: 10.1039/xoxxoooooox

www.rsc.org/

A new metal borohydride ammoniate (MBA), $Zr(BH_4)_4{\cdot}8NH_3$ was synthesized via ammoniation of $Zr(BH_4)_4$ crystal. The $Zr(BH_4)_4{\cdot}8NH_3$ has a distinctive structure and the highest coordination number of NH_3 groups among all the known MBAs. This compound could quickly dehydrogenate at 130 °C, enabling it a potential hydrogen storage material.

Hydrogen is considered as a clean and renewable energy carrier owing to its high energy density, lightweight and environmentally benign products of oxidation, making it a potential candidate to be used as a replacement for fossil fuels.[1-3] However, in order to utilize hydrogen for automotive applications, the greatest challenge is to develop safe, inexpensive, lightweight and high hydrogen content hydrogen storage materials that operate at moderate temperatures.[4, 5] Alkali and alkali-earth metal borohydrides, e.g., $LiBH_4$, $Mg(BH_4)_2$ and $Ca(BH_4)_2$, have received a lot of attention as potential candidates hydrogen storage materials due to their high gravimetric and volumetric hydrogen capacity.[6-13] Unfortunately, these candidates are unsuitable for proton exchange membrane fuel cell (PEMFC) applications, owing to their high hydrogen desorption temperatures and slow dehydrogenation kinetics.[14] Thus, new types of material with favorable dehydrogenation properties are in demand for promoting the development of current hydrogen storage technology.

Recently, first-principle calculations and experiments have demonstrated that the dehydrogenation temperature of metal borohydrides, $M(BH_4)_n$ (M = Li, Na, K, Cu, Mg, Zn, Sc, Zr, Hf, and so on), decreases with the increasing electronegativity (χ_p) of the metal cations.[15-17] The transition metal borohydrides contain metals with high values of χ_p. However, most of them are unstable or highly volatile at ambient conditions, such as $Ti(BH_4)_3$, $V(BH_4)_3$ and $Fe(BH_4)_3$.[18, 19] Furthermore, diborane is released upon the dehydrogenation process, which hinders the application of these metal borohydrides as solid hydrogen storage materials. Recent studies demonstrated that the unstable or highly volatile metal borohydrides can be turned into the stable metal borohydride ammoniates (MBAs) by interaction with ammonia.[20-25] Moreover, the protic N–H and hydridic B–H co-exist in their structures, which promotes the MBAs to dehydrogenate through a simple recombination of the $N–H^{\delta+}\cdots B–H^{\delta-}$, resulting in suppressing the release of diborane.[26-33]

In addition, our recent work has confirmed that the relationship between the χ_p of the central metal and the dehydrogenation properties is also applicable in MBAs.[20, 23, 26, 27, 34] Therefore, the Pauling electronegativity, χ_p, of the metal cation serves as a good indicator to estimate the dehydrogenation behaviors of MBAs. According to this rule, zirconium borohydride ammoniates should have a low dehydrogenation temperature due to the high electronegativity of Zr (χ_p = 1.4). However, $Zr(BH_4)_4$ is unstable and volatile under ambient conditions, which is not beneficial for collection and conservation.[18, 35, 36]

In this work, a facile ball-milling approach was applied to synthesize the solid-state $Zr(BH_4)_4$ crystal. The $Zr(BH_4)_4$ was ammoniated at once to form its octaammoniate, $Zr(BH_4)_4{\cdot}8NH_3$, which has a theoretical hydrogen capacity of 14.8 wt. %. Moreover, the structure of $Zr(BH_4)_4{\cdot}8NH_3$ was determined for the first time and shows a big difference of other reported metal borohydride ammoniates. This compound shows favorable dehydrogenation performance, enabling it to be a potential hydrogen storage material.

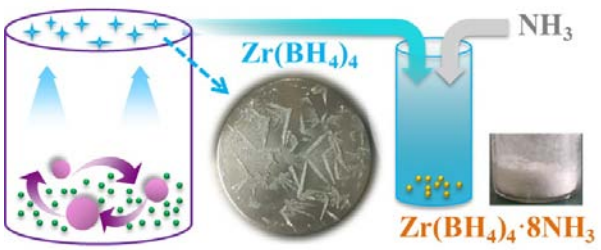

Scheme 1. A schematic illustration of the preparation of $Zr(BH_4)_4{\cdot}8NH_3$.

As illustrated in Scheme 1, a mixture of $LiBH_4$ and $ZrCl_4$ powders were ball milled using a conventional ball mill pot and operated at relative ambient temperature (< 20 °C), then the solvent-free $Zr(BH_4)_4$ crystals were synthesized through a cation exchange reaction in the solid-phase. Due to the volatility of $Zr(BH_4)_4$, the sublimated $Zr(BH_4)_4$ would separate with LiCl and deposit on the lid of ball mill pot directly during the ball milling process, then the target product $Zr(BH_4)_4{\cdot}8NH_3$ was easily fabricated by exposing the

$Zr(BH_4)_4$ crystal to an atmosphere of anhydrous ammonia in an ice-water bath. The as-obtained products were confirmed by elemental analysis, which gave a ratio of Zr:B:N = 1:4:8, and was measured using high-resolution XRD. In the XRD patterns (Fig. S1), new peaks were detected along with the disappearance of the peaks corresponding to the starting materials $LiBH_4$ and $ZrCl_4$, indicating that the metathesis and ammoniation reactions proceeded successfully and a new substance was obtained.

The XRD pattern at room temperature can be indexed with an orthorhombic unit cell using DICVOL06.[37] The structure solution was started using the charge-flipping algorithm implemented in the program TOPAS v4.2. One Zr atom was easily located in the electron density maps. The structure was subsequently solved in the space group of Pbca (No. 61) by global optimization in direct space with BH_4 and NH_3 groups as rigid bodies, using the program TOPAS v4.2 [38] and FOX [39] independently. Rietveld refinement was performed using TOPAS v4.2, and the refined lattice parameters are a = 16.76181(28) Å, b = 14.26414(26) Å, c = 13.65708(24) Å, V = 3265.309(98) $Å^3$. The diffraction profile fit by Rietveld refinement using these parameters is shown in Fig. S1, with the agreement factors *R*wp = 6.62%, R_B = 4.41%, and *Go*F =1.329. Furthermore, due to XRD not being sensitive to H atoms, the most stable structure and favorable positions of the hydrogen atoms in $Zr(BH_4)_4{\cdot}8NH_3$ were identified using first-principle calculations. The details of the structure determination and crystallographic data are presented in Table S1 and Table S2. The optimized crystal structure of $Zr(BH_4)_4{\cdot}8NH_3$ is shown in Fig. 1

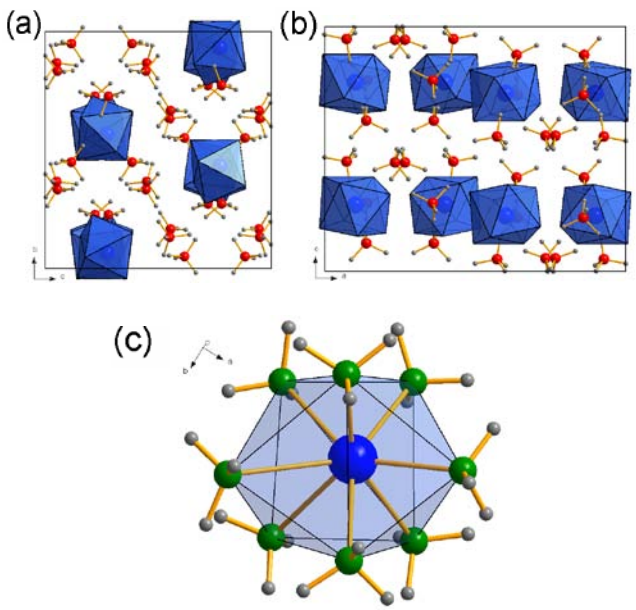

Fig. 1 Crystal structure of $Zr(BH_4)_4{\cdot}8NH_3$ as optimized by DFT and viewed along the (a) *a*-axis and (b) *b*-axis, showing the packing of $Zr(NH_3)_8$ side-bicapped trigonal prisms and BH_4 tetrahedra. (c) Local coordination of Zr with eight NH_3 molecules in the form of side-bicapped trigonal prism.

$Zr(BH_4)_4{\cdot}8NH_3$ has a distinctive structure from other reported MBAs and the highest coordination number of NH_3 groups among all known MBAs. There is one symmetry independent Zr atom in the unit cell coordinated with eight NH_3 molecules forming $Zr[NH_3]_8$ side-bicapped trigonal prism with a Zr–N bond distances of 2.15–2.67 Å (Fig. 1). Such coordination can be found in some fluorides of Zr such as Ba_2ZrF_8 [40] and telurides of Zr such as $ZrTe_5$.[41] The $Zr[NH_3]_8$ side-bicapped trigonal prism are packed in *ab*-layers in a hexagonal pattern which are then stacked along the *c*-axis (Fig. 1a, b). The BH_4 tetrahedra fill the empty space between the prisms in and between the *a*,*b*-layers. A dense network of di-hydrogen contacts shorter than 2.1 Å between NH_3 and BH_4 groups stabilizes the structure.

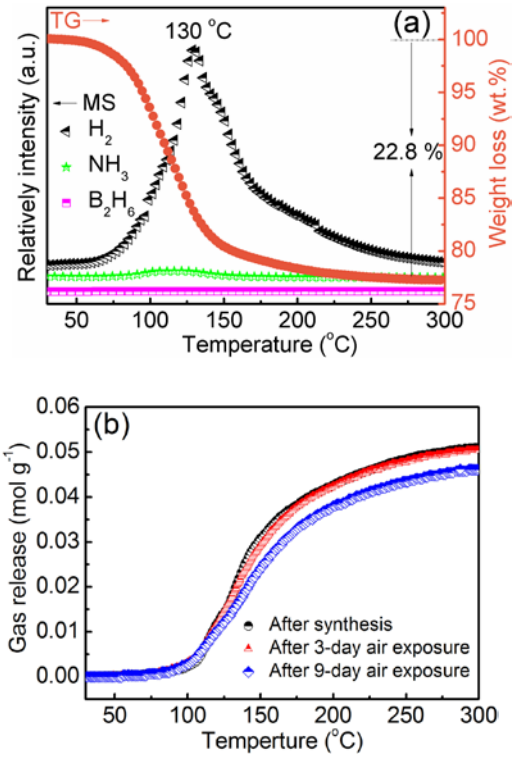

Fig. 2. (a) MS and TG profiles of $Zr(BH_4)_4{\cdot}8NH_3$; (b) TPD results for $Zr(BH_4)_4{\cdot}8NH_3$. All these measurements were performed with a heating rate of 5 °C min^{-1} under an atmosphere of argon.

The dehydrogenation properties of the $Zr(BH_4)_4{\cdot}8NH_3$ system were investigated by TG–MS (Fig. 2a) and TPD (Fig. 2b). A single hydrogen desorption process peaked at 130 °C was observed, accompanied with an emission of a small amount of ammonia. No B_2H_6 evolution was detected over the measured temperature range. The emission of ammonia can be ascribed to the surplus NH_3 groups related to the BH_4 groups in $Zr(BH_4)_4{\cdot}8NH_3$. A total weight loss of 22.8 wt. % at 300 °C was attributed to the combined release of H_2 and NH_3, as shown in the TG curve. The quantitative gas desorption of this system was determined using TPD measurements, which show that only a single hydrogen desorption step occurs, which is in accordance with the MS results. After heating $Zr(BH_4)_4{\cdot}8NH_3$ to 300 °C, 0.051 mol g^{-1} of gas was released. The purity of the hydrogen released was calculated to be 83.7 mol. %, according the equation combining the TG and volumetric desorbed gas results. The dehydrogenation kinetic properties of $Zr(BH_4)_4{\cdot}8NH_3$ were determined by investigating the isothermal hydrogen desorption curves (Fig. S2a). At 90 °C and 110 °C, around 4.8 wt. % and 6.1 wt. % hydrogen were released in 360 min. Upon elevating the heating temperature to 130 °C and 150 °C, 7.6 wt. % and 8.5 wt. % hydrogen were released within 360 min. The dehydrogenation capacity and purity at different temperatures are summarized and shown in Fig. S2b. Moreover, the gas release showed no change after 3 days and only a little decrease from 0.051 to 0.046 mol g^{-1} after 9 days of exposure to air at room temperature (Fig. 2b),

indicating its impressive air stability. In addition, it is noteworthy that no material expansion and foaming were observed, which is a problem suffered by many other B–N–H systems upon decomposition (Fig. S3).

To clarify the reaction mechanism for the as-obtained compounds, high-resolution synchrotron *in-situ* XRD, and Fourier transform infrared (FT-IR) and ^{11}B NMR spectroscopy were conducted. The high-resolution *in-situ* XRD results of $Zr(BH_4)_4{\cdot}8NH_3$ at temperatures ranging from 40 to 260 °C are shown in Fig. S4. It can be observed that the intensity of the diffraction peaks gradually increases with the decrease of full width at half maximum (FWHM) for the $Zr(BH_4)_4{\cdot}8NH_3$ phase upon heating the sample to 60 °C under an atmosphere of argon, indicating that the crystallinity of the sample increases as the temperature increased. Upon increasing the temperature further, the intensity of the peaks gradually reduces, and the sample transformed into an amorphous structure at 130 °C, which resulted from the decomposition of $Zr(BH_4)_4{\cdot}8NH_3$. The temperature for complete phase transformation in the *in-situ* XRD results is lower than that in the TG–MS results (Fig. 2). This was attributed to the slower heating rate and the long holding period (8 min for each pattern) during the *in-situ* measurements.

The FT-IR results shown in Fig. 3a reveals that the stretching and bending bands of the B–H bonds in the regions between 2180–2470 cm^{-1} and 1000–1280 cm^{-1} are present in $Zr(BH_4)_4{\cdot}8NH_3$ at room temperature. In addition, the vibrations assigned to the stretching of N–H bonds in a broad region ranging from 2950–3330 cm^{-1} and the bending of N–H bonds at 1405 cm^{-1} are observed. The bending of B–N bonds at 704 cm^{-1} is also observed, which may be due to the decomposition of a small amount of $Zr(BH_4)_4{\cdot}8NH_3$ during the measurement, resulting from the low onset dehydrogenation temperature of this compound. After heating to 130 °C, the intensity of the N–H and B–H absorptions is reduced equally while the vibrations that are attributed to B–N absorptions become stronger. This suggests that hydrogen release originates from a combination of the B–H and N–H species, resulting in the generation of B–N containing solid residues. Upon heating to 300 °C, the vibrations corresponding to the N–H and B–H absorptions completely disappear and only those associated with the B–N absorptions remain, which implies that the dehydrogenation reaction of $Zr(BH_4)_4{\cdot}8NH_3$ was complete at this temperature, as verified by the previous TG–MS results (Fig. 2).

The ^{11}B NMR spectra of $Zr(BH_4)_4{\cdot}8NH_3$ are presented in Fig. 3b. The peak centered at δ = –32.5 ppm corresponds to BH_4 and the weak peak centered at δ = –21.9 ppm attributed to BH_3, which may be due to the decomposition of a small quantity of $Zr(BH_4)_4{\cdot}8NH_3$ during the NMR acquisition. As the dehydrogenation temperature was increased to 130 °C, the peak corresponding to BH_4 is reduced while the peak attributed to BH_3 increases, accompanied with the appearance of new peaks at δ = –14.9, 1.4, 13.7 and 25.0 ppm, indicating the partial decomposition of the BH_4 group and the formation of BH_2, BH and B–N bonds upon the dehydrogenation process. After dehydrogenation at 300 °C, all the peaks assigned to BH_4, BH_3, BH_2 and BH bonds disappear and only the peaks corresponding to B–N bonds are observed, confirming the analysis of the FT-IR spectra. Due to the dehydrogenation of $Zr(BH_4)_4{\cdot}8NH_3$ is based on the combination of the $N–H^{\delta+}\cdots B–H^{\delta-}$, the dehydrogenated products could not be recharged with hydrogen directly.

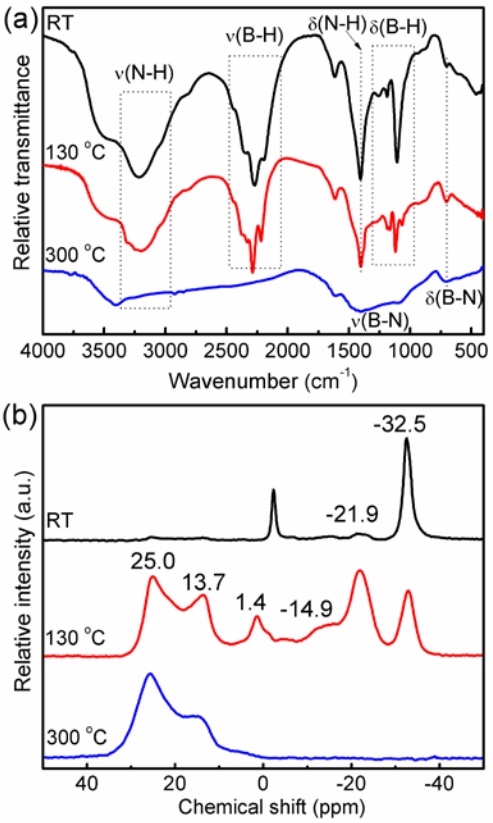

Fig. 3. (a) FT-IR spectra and (b) ^{11}B NMR spectra for $Zr(BH_4)_4{\cdot}8NH_3$ acquired at various temperatures.

Conclusions

In summary, $Zr(BH_4)_4$ was successfully synthesized using a facile solvent-free ball milling approach, and a subsequent ammoniation process was used to prepare its octaammoniate $Zr(BH_4)_4{\cdot}8NH_3$. The structure of $Zr(BH_4)_4{\cdot}8NH_3$ shows that Zr is coordinated by eight NH_3 molecules in the form of side-bicapped trigonal prism which are packed in *a,b*-layers of the orthorhombic structure. The BH_4 tetrahedra fill the empty space between the prisms in and between the *a,b*-layers. This compound starts to release hydrogen at 60 °C with a dehydrogenation peak centered at 130 °C. Further improvement on the hydrogen release purity and kinetic can be achieved via combination of metal borohydrides or nanoconfinemnt in scaffold, which are underway and will be reported in our latter work.

This work was partially supported by the National Natural Science Foundation of China (Nos. U1201241, 51271078, 21271046 and 51471053), GDUPS (2014), and Guangxi Collaborative Innovation Center of Structure and Property for New Energy and Materials. Part of this research was undertaken on the Powder Diffraction beamline at the Australian Synchrotron, Victoria, Australia.

Notes and references

[a] School of Materials Science and Engineering and Key Laboratory of Advanced Energy Storage Materials of Guangdong Province, South China University of Technology, Guangzhou 510641, China. Email: meouyang@scut.edu.cn

[b] Department of Materials Science, Fudan University, Shanghai 200433, China. Email: yuxuebin@fudan.edu.cn

[c] Australian Synchrotron, 800 Blackburn Rd., Clayton 3168, Australia.

[d] Laboratoire de Cristallographie, DQMP, Université de Genève, Genève 1211, Switzerland

Electronic Supplementary Information (ESI) available: [Experiment and crystallographic details, calculated atomic coordination, isothermal dehydrogenation of $Zr(BH_4)_4{\cdot}8NH_3$. Photograph of the $Zr(BH_4)_4{\cdot}8NH_3$ before and after dehydrogenation.]. See DOI: 10.1039/c000000x/

1. L. Schlapbach and A. Zuttel, *Nature*, 2001, **414**, 353-358.
2. K. J. Jeon, H. R. Moon, A. M. Ruminski, B. Jiang, C. Kisielowski, R. Bardhan and J. J. Urban, *Nat. Mater.*, 2011, **10**, 286-290.
3. A. Züttel, *Mater. Today*, 2003, **6**, 24-33.
4. E. Y. Marrero-Alfonso, A. M. Beaird, T. A. Davis and M. A. Matthews, *Ind. Eng. Chem. Res.*, 2009, **48**, 3703-3712.
5. T. K. Nielsen, F. Besenbacher and T. R. Jensen, *Nanoscale*, 2011, **3**, 2086-2098.
6. H.-W. Li, Y. Yan, S.-i. Orimo, A. Züttel and C. M. Jensen, *Energies*, 2011, **4**, 185-214.
7. P. Chen and M. Zhu, *Mater. Today*, 2008, **11**, 36-43.
8. S.-i. Orimo, Y. Nakamori, J. R. Eliseo, A. Züttel and C. M. Jensen, *Chem. Rev.*, 2007, **107**, 4111-4132.
9. C. Li, P. Peng, D. W. Zhou and L. Wan, *Int. J. Hydrogen Energy*, 2011, **36**, 14512-14526.
10. H. Hagemann and R. Cerny, *Dalton T.*, 2010, **39**, 6006-6012.
11. J. Huang, Y. Yan, L. Ouyang, H. Wang, J. Liu and M. Zhu, *Dalton T.*, 2014, **43**, 410-413.
12. Y. Yan, A. Remhof, D. Rentsch and A. Zuttel, *Chem Commun*, 2015. DOI: 10.1039/c4cc05266h
13. M. A. Wahab, Y. A. Jia, D. Yang, H. Zhao and X. Yao, *J Mater. Chem. A*, 2013, **1**, 3471-3478.
14. C. Weidenthaler and M. Felderhoff, *Energy Environ. Sci.*, 2011, **4**, 2495-2502.
15. Y. Nakamori, H. W. Li, M. Matsuo, K. Miwa, S. Towata and S. Orimo, *J. Phys. Chem. Solids*, 2008, **69**, 2292-2296.
16. Y. Nakamori, K. Miwa, A. Ninomiya, H. Li, N. Ohba, S.-i. Towata, A. Züttel and S.-i. Orimo, *Phys. Rev. B*, 2006, **74**, 045126.
17. H. W. Li, S. Orimo, Y. Nakamori, K. Miwa, N. Ohba, S. Towata and A. Züttel, *J. Alloy Compd.*, 2007, **446–447**, 315-318.
18. H. R. Hoekstra and J. J. Katz, *J. Am. Chem. Soc.*, 1949, **71**, 2488-2492.
19. T. J. Marks and J. R. Kolb, *Chem. Rev.*, 1977, **77**, 263-293.
20. Y. Guo, X. Yu, W. Sun, D. Sun and W. Yang, *Angew. Chem. Int. Ed.*, 2011, **50**, 1087-1091.
21. F. Yuan, Q. Gu, X. Chen, Y. Tan, Y. Guo and X. Yu, *Chem. Mater.*, 2012, **24**, 3370-3379.
22. Z. Tang, F. Yuan, Q. Gu, Y. Tan, X. Chen, C. M. Jensen and X. Yu, *Acta Mater.*, 2013, **61**, 3110-3119.
23. Q. F. Gu, L. Gao, Y. H. Guo, Y. B. Tan, Z. W. Tang, K. S. Wallwork, F. W. Zhang and X. B. Yu, *Energy Environ. Sci.*, 2012, **5**, 7590-7600.
24. M. Li, F. Yuan, Q. Gu and X. Yu, *Int. J. Hydrogen Energy*, 2013, **38**, 9236-9242.
25. L. Li, J. Huang, M. Li, Q. Li, L. Ouyang, M. Zhu and X. Yu, *Int. J. Hydrogen Energy*, 2013, **38**, 16208-16214.
26. Y. Guo, G. Xia, Y. Zhu, L. Gao and X. Yu, *Chem. Commun.*, 2010, **46**, 2599-2601.
27. G. Soloveichik, J.-H. Her, P. W. Stephens, Y. Gao, J. Rijssenbeek, M. Andrus and J. C. Zhao, *Inorg. Chem.*, 2008, **47**, 4290-4298.
28. Z. Tang, Y. Tan, Q. Gu and X. Yu, *J. Mater. Chem.*, 2012, **22**, 5312-5318.
29. X. Zheng, G. Wu, W. Li, Z. Xiong, T. He, J. Guo, H. Chen and P. Chen, *Energy Environ. Sci.*, 2011, **4**, 3593-3600.
30. G. Xia, Q. Gu, Y. Guo and X. Yu, *J. Mater. Chem.*, 2012, **22**, 7300-7307.
31. Y. Yang, Y. Liu, H. Wu, W. Zhou, M. Gao and H. Pan, *Phys. Chem. Chem. Phys.*, 2014, **16**, 135-143.
32. Y. Yang, Y. Liu, Y. Li, M. Gao and H. Pan, *J. Phys. Chem. C*, 2013, **117**, 16326-16335.
33. L. H. Jepsen, M. B. Ley, Y.-S. Lee, Y. W. Cho, M. Dornheim, J. O. Jensen, Y. Filinchuk, J. E. Jørgensen, F. Besenbacher and T. R. Jensen, *Mater. Today*, 2014, **17**, 129-135.
34. H. Chu, G. Wu, Z. Xiong, J. Guo, T. He and P. Chen, *Chem. Mater.*, 2010, **22**, 6021-6028.
35. W. E. Reid, J. M. Bish and A. Brenner, *J. Electrochem. Soc.*, 1957, **104**, 21-29.
36. F. C. Gennari, L. Fernández Albanesi and I. J. Rios, *Inorg. Chim. Acta*, 2009, **362**, 3731-3737.
37. A. Boultif and D. Louer, *J. Appl. Crystallogra.*, 2004, **37**, 724-731.
38. A. Bruker, *User's Manual, Bruker AXS, Karlsruhe, Germany*, 2005.
39. V. Favre-Nicolin and R. Cerny, *J. Appl. Crystallogra.*, 2002, **35**, 734-743.
40. A. Le Bail and J.-P. Laval, *Eur. J. Solid State Inorg. Chem.*, 1998, **35**, 357-372.
41. H. Fjellvåg and A. Kjekshus, *Solid State Commun.*, 1986, **60**, 91-93.

